

Critical exponents near the Liouvillian exceptional structure in Rydberg vapors

Chuanming Li(李传铭), Konghao Sun(孙孔浩), and Wei Yi(易为)

Citation: Chin. Phys. B, 2026, 35 (**3**): 030302. DOI: 10.1088/1674-1056/adfb57
http://cpb.iphy.ac.cn; http://iopscience.iop.org/cpb

What follows is a list of articles you may be interested in

Dynamical evolution of imaginarity resources in non-Markovian environments

Hong-Biao Li(李宏彪), Deng-Guo Kong(孔德国), Xue-Ping Chai(柴学平), Jin-Long Yu(余金龙), and Qiang Zheng(郑强)

Chin. Phys. B, 2025, 34 (**11**): 110309. DOI: 10.1088/1674-1056/ade4b1

Quantum interferometric power and non-Markovianity in the decoherence channels

Shaojie Xiong(熊少杰), Zhe Sun(孙哲), and Xiaoguang Wang(王晓光)

Chin. Phys. B, 2023, 32 (**8**): 080302. DOI: 10.1088/1674-1056/accb4e

Non-Markovianity of an atom in a semi-infinite rectangular waveguide

Jing Zeng(曾静), Yaju Song(宋亚菊), Jing Lu(卢竞), and Lan Zhou(周兰)

Chin. Phys. B, 2023, 32 (**3**): 030305. DOI: 10.1088/1674-1056/acac18

Floquet scattering through a parity-time symmetric oscillating potential

Xuzhen Cao(曹序桢), Zhaoxin Liang(梁兆新), and Ying Hu(胡颖)

Chin. Phys. B, 2023, 32 (**3**): 030302. DOI: 10.1088/1674-1056/aca39a

Two-body exceptional points in open dissipative systems

Peize Ding(丁霈泽) and Wei Yi(易为)

Chin. Phys. B, 2022, 31 (**1**): 010309. DOI: 10.1088/1674-1056/ac3396

Critical exponents near the Liouvillian exceptional structure in Rydberg vapors

Chuanming Li(李传铭)[1], Konghao Sun(孙孔浩)[2,†], and Wei Yi(易为)[1,3,4,5]

[1] *Laboratory of Quantum Information, University of Science and Technology of China, Hefei* 230026, *China*
[2] *Beijing National Laboratory for Condensed Matter Physics, Institute of Physics, Chinese Academy of Sciences (CAS), Beijing* 100190, *China*
[3] *Anhui Province Key Laboratory of Quantum Network, University of Science and Technology of China, Hefei* 230026, *China*
[4] *CAS Center For Excellence in Quantum Information and Quantum Physics, Hefei* 230026, *China*
[5] *Anhui Center for Fundamental Sciences in Theoretical Physics, University of Science and Technology of China, Hefei* 230026 *China*

(Received 9 June 2025; revised manuscript received 24 July 2025; accepted manuscript online 14 August 2025)

In a dissipative Rydberg vapor, the interplay of many-body effects and non-Hermiticity gives rise to a Liouvillian exceptional structure, where exceptional arcs merge at a higher-order exceptional point of the Liouvillian superoperator. Spectral features of the exceptional structure naturally give rise to critical dynamics, which have interesting implications for experiments. In this work, we study the response of the system to perturbations near the Liouvillian exceptional structure, and evaluate the critical exponents. The results are consistent with those in linear non-Hermitian Hamiltonians, thus confirming the exceptional nature of the structures herein. We also discuss how these exponents can be measured experimentally.

Keywords: Rydberg vapors, open system, Liouvillian exceptional point, critical scaling

PACS: 03.65.Yz, 05.70.Jk, 42.50.–p, 05.30.Rt

DOI: 10.1088/1674-1056/adfb57 **CSTR:** 32038.14.CPB.adfb57

1. Introduction

The exceptional points (EPs) are the branch-point singularities in non-Hermitian systems, which have attracted extensive interest in recent years.[1–5] At an n-th-order EP, a number of n eigenvalues and eigenvectors of the underlying non-Hermitian Hamiltonian coalesce, and the Hamiltonian becomes non-diagonalizable.[6–10] The singularity is characterized by a topological invariant,[11–16] and hosts critical and topological behaviors, such as the emergence of critical exponents,[17–28] and the chiral model switching.[29–41] Besides non-Hermitian Hamiltonians, which are often implemented experimentally in the conditional quantum dynamics of open systems, these singularities also arise in the unconditional dynamics of open systems, wherein the time evolution of the density matrix is driven by the Liouvillian superoperator. Therein, exceptional structure have been identified in the Liouvillian eigenspectrum.[42–45] An outstanding manifestation is the internal-state dynamics of a dissipative Rydberg vapor, where the presence of an exceptional structure can be identified in the Liouvillian spectrum.[46,47] Therein, two second-order exceptional arcs merge into a third-order EP. Crucially, the Liouvillian of the system features a non-linear coherent Hamiltonian, which originates from the many-body effects under the mean-field approximation.[48–54] Under the double-space formalism with a vectorized density matrix, the Liouvillian is mapped to a non-linear non-Hermitian Hamiltonian, giving rise to the non-linear exceptional structures. While signatures of the exceptional dynamics and chiral state transfer have been experimentally observed in such a system,[46] the critical behavior of the non-linear Liouvillian ES remains unclarified.

In this work, we analytically derive the critical exponents of the Liouvillian ES in dissipative Rydberg gases. This entails the study of the response of the system to small perturbations along different directions across the exceptional structures. While the ES herein is composed to two second-order exceptional arcs merging at a third-order EP, we find that the critical exponent is $1/2$ near the second-order exceptional arc. By contrast, the exponent is $1/3$ when crossing the third-order EP, except when the perturbation is performed along a special symmetry line. These findings agree with a previous study on the critical behaviors of bistability transition in Rydberg gases, and are consistent with existing studies of exceptional structures in linear non-Hermitian systems. Finally, we discuss potential experimental signals for the critical exponents, taking into account the finite resolution of the imposed perturbations.

The work is organized as follows. In Section 2, we review the setup and modeling of the dissipative Rydberg gas, as well as the Liouvillian ES therein. We then study the critical exponents near the exceptional structure in Section 3, both analytically and numerically. In Section 4, we discuss potential experimental signals of the critical exponents. We summarize

†Corresponding author. E-mail: sunkh@iphy.ac.cn

© 2026 Chinese Physical Society and IOP Publishing Ltd. All rights, including for text and data mining, AI training, and similar technologies, are reserved.

in Section 5.

2. Rydberg vapor and Liouvillian EP

We consider a dissipative Rydberg vapor at room temperature. As illustrated in Fig. 1, the electronic ground state of the atom, denoted as $|1\rangle$, is off-resonantly coupled to the Rydberg state $|2\rangle$ by lasers (in a typical two-photon process, but simplified to a single effective Rydberg excitation field with Rabi frequency Ω here). The Rydberg state features a decay rate Γ to the ground state, which can be tuned by coupling the state $|2\rangle$ to other excited states which eventually decay to the ground state $|1\rangle$. For simplicity, we neglect the dephasing between the ground and Rydberg state here (which does not qualitatively change our conclusions). Atoms in the Rydberg state interact with each other through the long-range Rydberg interaction, which is approximated by a constant all-to-all coupling rate V. This approximation is widely adopted for the description of Rydberg vapors.[48–54]

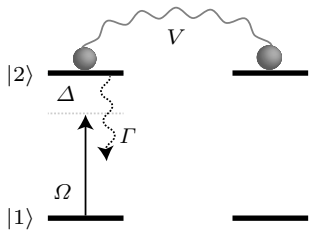


Fig. 1. Schematics of the system. The states $|1\rangle$ and $|2\rangle$ represent the ground and Rydberg states, respectively. The parameter Ω denotes the effective coupling strength between the ground state and the Rydberg state, while Δ represents the detuning. The decay rate of the Rydberg state is denoted by Γ, and V signifies the interaction strength between Rydberg atoms.

The coherent Hamiltonian of the system is given by

$$H = \Omega \sum_k \hat{\sigma}_k^x + \left(\Delta - V \sum_p \hat{n}_p\right) \sum_k \hat{n}_k, \tag{1}$$

where $\hat{\sigma}_k^x = |1\rangle\langle 2| + |2\rangle\langle 1|$ of the k-th atom, and $\hat{n}_k$ is the Rydberg-state occupation of the k-th atom. The quantum jump operator associated with the decay process is

$$L_k = \sqrt{\Gamma} \frac{\hat{\sigma}_k^x - \mathrm{i}\hat{\sigma}_k^y}{2}, \tag{2}$$

where the Pauli operator $\hat{\sigma}_k^y$ is defined in the two-dimensional state space $\{|1\rangle, |2\rangle\}$ of the kth atom. Under the mean-field approximation, each individual atom is decoupled from the ensemble except for a nonlinear detuning term, the density matrix can be written as $\rho = \bigotimes_k \bar{\rho}$, and the optical Bloch equations can be re-arranged into the equations of motion of the average spin and Rydberg-state occupation

$$\dot{S}^x = -\frac{\Gamma}{2} S^x - (\Delta + nV) S^y, \tag{3}$$

$$\dot{S}^y = (\Delta + nV) S^x - \frac{\Gamma}{2} S^y - 4\Omega n + 2\Omega, \tag{4}$$

$$\dot{n} = \Omega S^y - \Gamma n, \tag{5}$$

where $S^j = \mathrm{Tr}(\bar{\rho}\hat{\sigma}_k^j)$ $(j = x, y, z)$ and $n = \mathrm{Tr}(\bar{\rho}\hat{n}_k)$. Note that the optical Bloch equation and the equations of motion of the spin operators, are equivalent to the master equation $\dot{\rho} = \mathcal{L}[\rho]$, where $\mathcal{L}$ is the Liouvillian superoperator associated with coherent Hamiltonian (1) and jump operators (2).

We are interested in the steady state, which is solved by setting the time derivatives on the left-hand side of the equations above to zero. This leads to the equation

$$V^2 n^3 + 2\Delta V n^2 + \left(2\Omega^2 + \frac{\Gamma^2}{4} + \Delta^2\right) n - \Omega^2 = 0, \tag{6}$$

Since the steady states can also be solved by requiring $\mathcal{L}[\rho] = 0$, the solutions of Eq. (6) reflect the steady-state sector (with zero Liouvillian eigenvalue) of the Liouvillian spectrum.

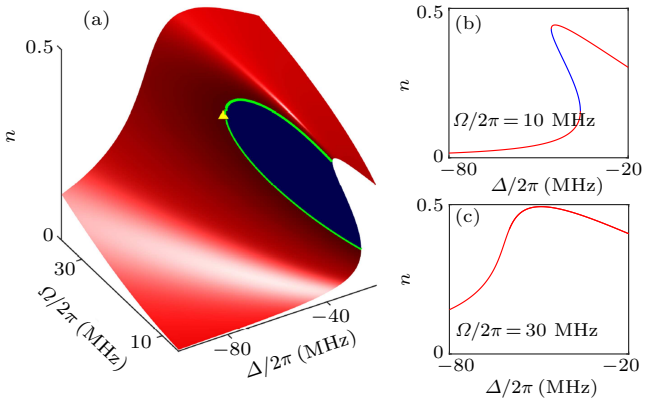


Fig. 2. The Rydberg-state occupation in the steady states. (a) Rydberg-state occupation n as a function of Ω and Δ. The stable steady-state solutions are represented by the red region, while unstable steady-state solutions are indicated by the blue region. The second-order exceptional arcs are marked by green curves, with their intersection marked by a yellow triangle, denoting the third-order EP. (b)–(c) Rydberg-state occupation as a function of Δ, with $\Omega/2\pi$ fixed at 10 MHz and 30 MHz, respectively. Other parameters are: $\Gamma/2\pi = 10$ MHz, $V/2\pi = 100$ MHz.

In Fig. 2(a), we show a typical steady-state solution of the system, with the Rydberg-state occupation as a function of Δ and Ω. While the red-shaded region corresponds to stable steady-state solutions, the blue-shaded region corresponds to unstable solutions. From the cross-section view in Fig. 2(b), we see that a bistable region exists where two stable solution coexist with an unstable solution. This structure gives rise to the well-studied bistable transitions and hysteresis behaviors of the Rydberg gas. However, from the perspective of the Liouvillian superoperator, the structure also corresponds to a non-linear ES. Explicitly, along the green curve in Fig. 2(a), one of the two stable steady states and the unstable steady state coalesce. This is the second-order exceptional arc. At the point marked by the yellow triangle in Fig. 2(a), all three steady states coalesce, which is identified as the third-order EP. The overall ES in Fig. 2(a) can thus be understood as two exceptional arcs (the upper and lower branch green curves) merging at the EP. Note that such a structure is also present in non-linear non-Hermitian systems, which have attracted much interest of late.[55–57] Furthermore, in a previous study, chiral steady-state transfer is experimentally demonstrated using

Rydberg vapors,[46] based on the non-Hermitian perspective of the system reviewed above.

3. Critical exponents

An outstanding feature of the EPs is their sensitivity to external perturbations. At the n-th-order EP for instance, a small perturbation of the order ε can lead to a change in the eigenspectrum, which is of the order $\varepsilon^{1/n}$. Here the fractional exponent $1/n$ is referred to as the critical exponent. Since the nonlinear exceptional structure observed above is defined based on the eigenspectrum degeneracy, a natural question is whether similar critical exponents can be observed.

To study the critical exponent, we follow the practice in Ref. [49], and define the dimensionless variables

$$a = 2+\frac{1}{4}\frac{\Gamma^2}{\Omega^2}, \tag{7}$$

$$b = \frac{V^2}{\Omega^2}, \tag{8}$$

$$c = \frac{\Delta}{V}, \tag{9}$$

so that equation (6) becomes

$$n[a+b(c+n)^2] = 1, \tag{10}$$

with $a \geq 2$, $b \geq 0$, and $c < 0$. We focus on the nontrivial case with $b > 0$.

More relevantly, the discriminant of Eq. (10) is

$$D = \left(\frac{a}{3b}-\frac{c^2}{9}\right)^3 + \left(\frac{1}{2b}+\frac{ac}{3b}+\frac{c^3}{27}\right)^2. \tag{11}$$

Hence, the equation hosts three real roots (three steady-state solutions) when $D \leq 0$. When $D = 0$, two of the three roots are equal, corresponding to solutions on the exceptional arc. Otherwise, when $D = 0$ and

$$\frac{a}{3b}-\frac{c^2}{9} = \frac{1}{2b}+\frac{ac}{3b}+\frac{c^3}{27} = 0,$$

all three solutions are equal, corresponding to the third-order EP.

In Fig. 3(a), we show the exceptional structure in the parameter space of (a,b), with a fixed parameter c. The green curves are the exceptional arcs, satisfying $D = 0$. And the third-order EP, or the critical point, is given by $(a_c, b_c) = (-9/(8c), -27/(8c^3))$. Furthermore, a symmetry line exists at the critical point, which is tangential to either of the exceptional arcs. It is straightforward to show that the slope of the symmetry line is $k_c = -9/c^2$.

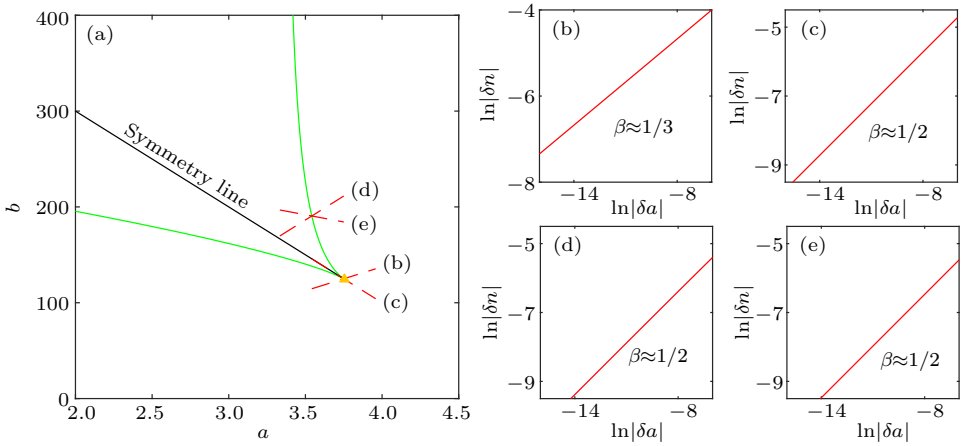


Fig. 3. Exceptional structure and scaling behavior. (a) Exceptional structure in the dimensionless parameter space of a and b. The green curves are the exceptional arcs, the yellow triangle denotes the third-order EP, and the black line denotes the symmetry line (see main text). (b)–(e) Scaling behavior of the Rydberg-state occupation in the vicinity of the ES along the paths labeled in panel (a). Here we fix $c = -0.3$.

We now investigate the critical exponent along the exceptional arc. Assuming (a_0, b_0, n_0) satisfy Eq. (10), we fix the parameter c, and perturb the system along the line $k = \delta b/\delta a$, with $(a_0+\delta a, b_0+\delta b, n_0+\delta n)$ still satisfying Eq. (10). We then have

$$\begin{aligned} &P\delta n + M\delta n^2 + b_0\delta n^3 \\ &+\delta a(Y + Q\delta n + N\delta n^2 + k\delta n^3) = 0, \end{aligned} \tag{12}$$

where

$$P = a_0 + b_0c^2 + 4b_0n_0c + 3b_0n_0^2, \tag{13}$$

$$M = 2b_0c + 3b_0n_0, \tag{14}$$

$$Y = n_0 + n_0(c+n_0)^2k, \tag{15}$$

$$Q = 1 + kc^2 + 4kn_0c + 3kn_0^2, \tag{16}$$

$$N = 2kc + 3kn_0. \tag{17}$$

Invoking the condition δa, δb, $\delta n \ll 1$, from Eq. (12), we derive the relation $|\delta n| \sim |\delta a|^\beta$, where β is the critical exponent. We list the results as follows:

$$P = 0,\ M = 0,\ Y \neq 0: \quad \beta = \frac{1}{3}, \tag{18}$$

$$P = 0,\ M = 0,\ Y = 0: \quad \beta = \frac{1}{2} \quad \text{or} \quad +\infty, \tag{19}$$

$$P = 0,\ M \neq 0,\ Y \neq 0: \quad \beta = \frac{1}{2}, \tag{20}$$

$$P = 0,\ M \neq 0,\ Y = 0: \quad \beta = 1 \quad \text{or} \quad +\infty, \tag{21}$$

$$P \neq 0,\ Y \neq 0: \quad \beta = 1, \tag{22}$$

$$P \neq 0,\ Y = 0: \qquad \beta = +\infty. \tag{23}$$

These analytic expressions are the main results of this work. Here P and M determine the position of (a_0, b_0), while Y determines k, the direction of perturbation. Specifically, the condition $P = 0$ means (a_0, b_0) is on the exceptional arc; $P = 0$, $M = 0$ means it is at the third-order EP; $P = 0$, $Y = 0$ means the direction of perturbation is tangential to the exceptional arc. When $Y = 0$, equation (12) clearly shows that $\delta n = 0$ is always a solution for this particular perturbation direction, and this solution is independent of δa. Consequently, for this branch of solution, the critical exponent is $\beta = +\infty$ [see Eqs. (19), (21), and (23)]. With these in mind, the analytical results above can be interpreted as follows. At the critical point (third-order EP), the critical exponent is $\beta = 1/2$ when the system is perturbed along the symmetry line [see Eq. (19)], the critical exponent is $\beta = 1/3$ otherwise [see Eq. (18)]. Along the exceptional arc (but not the critical point), the critical exponent is $\beta = 1/2$ [see Eq. (20)], so long as the system is not perturbed along the line tangential to the exceptional arc. Moreover, in the general case where $P \neq 0$, (a_0, b_0) is not an EP, and the exponent $\beta = 1$ [see Eq. (22)].

In Fig. 3(b), we perturb the system at different (a_0, b_0) along the red dashed lines in Fig. 3(a). The critical exponents are extracted by numerically fitting the response of the system $\ln|\delta n|$ to the perturbation $\ln|\delta a|$. Our numerical results are consist with the analytic derivations above.

The critical exponents we obtained are based on the mean-field approximation. However, it is known that in a realistic Rydberg atomic ensemble, the mean-field approximation is valid in parameter regimes far from the critical point but may fail to accurately describe the system's behavior near the critical point itself.[52] Therefore, we expect that the second-order exceptional arc defined by the phase boundary and its corresponding critical exponent $\beta = 1/2$ should still exist even when beyond-mean-field effects are considered. In contrast, the scaling behaviour at the critical point is more subtle, and whether its critical exponent agrees with the mean-field prediction is not straightforward that warrants further investigation.

4. Probing the critical point

Summarizing the results in the previous section, the critical exponent $\beta = 1/3$ is a unique feature of the critical point, but its emergence is strictly conditional on the proximity of the perturbed system to the critical point, and on the direction of the perturbation. Experimentally, this becomes demanding with the initial state preparation, and the limited resolution of the perturbation δa.

We consider two scenarios. First, one can prepare the system at the critical point and change the direction of perturbation. As shown in Fig. 4(a), a sharp jump from $\beta = 1/2$ to $\beta = 1/3$ occurs when the direction of perturbation aligns with that of the symmetry line. Importantly, the sharpness of the cusp at $k = k_c$ increases as the resolution of perturbation δa improves. Second, one can always perturb the system in the direction of the symmetry line, but varying the initial parameter $\{a_0, b_0\}$ along the exceptional arc. As illustrated in Fig. 4(b), the critical exponent dips sharply and approaches $1/3$ near the critical point $\Delta a_c = 0$. Here $\Delta a_c = a_0 - a_c$ is the distance between the critical point and initial point of perturbation. Again, the sharpness of the dip increases as the resolution of perturbation is improved. In either scenario, the critical exponent is numerically extracted by fitting the system response to perturbations in a. The latter, in discrete steps of δa, represents the achievable resolution. Hence, signals of the critical exponent and its variations can be extracted from measurements with finite-resolution perturbations.

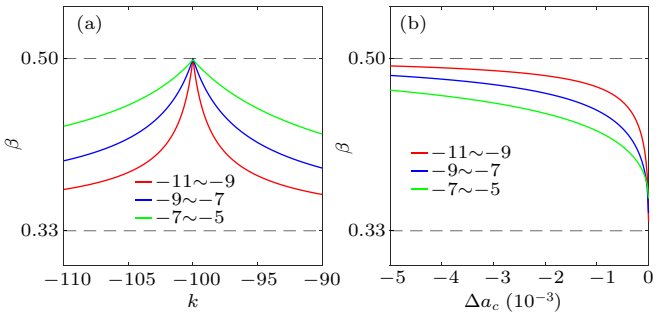


Fig. 4. Variation of the critical exponent. (a) Critical exponent as a function of k in the vicinity of the third-order EP. The curves, distinguished by their colors, represent various ranges of $\ln|\delta a|$ used for numerical evaluation (see legends). (b) Critical exponent as a function of Δa_c in the vicinity of the third-order EP. Here we take $c = -0.3$.

Figure 4(b) shows that under a finite-step perturbation, the fitted critical exponent decreases as the system approaches its critical point. This suggests an possible experimental method for locating the critical point: one could identify the parameter set that yields a minimum fitted exponent while keeping the perturbation step size fixed. In a typical three-level atom experiment,[48] this can be achieved by first obtaining the probe light's transmittance spectrum through a scan of a system parameter (e.g., probe detuning). Subsequently, one would calculate the critical exponent by fitting the transmittance data across a fixed perturbation step for various parameter settings. The primary limitation of this method is experimental noise, which restricts how small the perturbation step can be, thereby limiting the precision of locating the critical point.

Furthermore, based on a realistic experimental setup,[46] we can give the key parameters needed to test the theory. Specifically, for an Rb vapor cell with dimensions of 8 mm × 8 mm × 8 mm at $T = 70$ °C, the atomic density is $n_a = 6.3 \times 10^5$ m^{-3}. The probe light couples the $|5S_{1/2}\rangle$ and $|5P_{3/2}\rangle$ levels of ^{87}Rb, while the coupling light, with a power of $P_c = 127.3$ MW, resonantly couples the $|5P_{3/2}\rangle$ and $|50D_{5/2}\rangle$ levels

(corresponding to a Rabi frequency of $\Omega_c/2\pi = 12.21$ MHz). Under these conditions, in the parameter space defined by Rabi frequency of the probe light Ω_p and the coupling light detuning Δ_c, the critical point is located near $\Delta_c/2\pi = -4.77$ MHz and $\Omega_p/2\pi = 7.32$ MHz.

5. Summary

To summarize, we analytically derive the critical exponents for the Liouvillian ES in Rydberg vapors. Though nonlinear in nature, these critical exponents are qualitatively similar to their counterparts in linear non-Hermitian Hamiltonians. While our results offer further insight into the Liouvillian ES, they can also be useful for developing sensing schemes based on these ES in dissipative Rydberg gases. For future studies, it is desirable to explore the topological nature of the Liouvillian ES, and to look for ES containing higher-order EPs and more complex structures.

Acknowledgement

Project supported by the National Natural Science Foundation of China (Grant No. 12374479).

References

[1] Ashida Y, Gong Z and Ueda M 2020 *Adv. Phys.* **69** 249
[2] Miri M A and Alù A 2019 *Science* **363** 42
[3] Özdemir Ş K, Rotter S, Nori F and Yang L 2019 *Nat. Mater.* **18** 783
[4] Ding K, Fang C and Ma G 2022 *Nat. Rev. Phys.* **4** 745
[5] Li A, Wei H, Cotrufo M, Chen W, Mann S, Ni X, Xu B, Chen J, Wang J, Fan S, Qiu C W, Alù A and Chen L 2023 *Nat. Nanotech.* **18** 706
[6] Kato T 1966 *Perturbation Theory of Linear Operators* (Springer)
[7] Franklin J N 1993 *Matrix Theory* (Dover Publications)
[8] Heiss W D 1999 *Eur. Phys. J. D* **7** 1
[9] Berry M 2004 *Czech. J. Phys.* **54** 1039
[10] Heiss W D 2004 *J. Phys. A: Math. Gen.* **37** 2455
[11] Heiss W D 2000 *Phys. Rev. E* **61** 929
[12] Dembowski C, Gräf H D, Harney H L, Heine A, Heiss W D, Rehfeld H and Richter A 2001 *Phys. Rev. Lett.* **86** 787
[13] Dembowski C, Dietz B, Gräf H D, Harney H L, Heine A, Heiss W D and Richter A 2004 *Phys. Rev. E* **69** 056216
[14] Lee S B, Yang J, Moon S, Lee S Y, Shim J B, Kim S W, Lee J H and An K 2009 *Phys. Rev. Lett.* **103** 134101
[15] Gao T, Estrecho E, Bliokh K Y, Liew T C H, Fraser M D, Brodbeck S, Kamp M, Schneider C, Höfling S, Yamamoto Y, Nori F, Kivshar Y S, Truscott A G, Dall R G and Ostrovskaya E A 2015 *Nature* **526** 554
[16] Tang W, Ding K and Ma G 2021 *Phys. Rev. Lett.* **127** 034301
[17] Wiersig J 2016 *Phys. Rev. A* **93** 033809
[18] Chen W, Özdemir Ş K, Zhao G, Wiersig J and Yang L 2017 *Nature* **548** 192
[19] Ren J, Hodaei H, Harari G, Hassan A U, Chow W, Soltani M, Christodoulides D and Khajavikhan M 2017 *Opt. Lett.* **42** 1556
[20] Zhang M, Sweeney W, Hsu C W, Yang L, Stone A D and Jiang L 2019 *Phys. Rev. Lett.* **123** 180501
[21] Hokmabadi M P, Schumer A, Christodoulides D N and Khajavikhan M 2019 *Nature* **576** 70
[22] Wiersig J 2020 *Photon. Res.* **8** 1457
[23] Park J H, Ndao A, Cai W, Hsu L, Kodigala A, Lepetit T, Lo Y H and Kanté B 2020 *Nat. Phys.* **16** 462
[24] Li W, Zhou Y, Han P, Chang X, Jiang S, Huang A, Zhang H and Xiao Z 2021 *Phys. Rev. A* **104** 033505
[25] Jiang S, Xiao Z, Li W, Chen T, Li J, Huang A and Zhang H 2022 *J. Appl. Phys.* **131** 103106
[26] Carlo M D, Leonardis F D, Soref R A and Passaro V M N 2022 *J. Lightwave Technol.* **40** 6021
[27] Jiang H, Zhang W, Lu G, Ye L, Lin H, Tang J, Xue Z, Li Z, Xu H and Gong Q 2022 *Photon. Res.* **10** 557
[28] Kononchuk R, Cai J, Ellis F, Thevamaran R and Kottos T 2022 *Nature* **607** 697
[29] Latinne O, Kylstra N J, Dörr M, Purvis J, Terao-Dunseath M, Joachain C J, Burke P G and Noble C J 1995 *Phys. Rev. Lett.* **74** 46
[30] Lefebvre R, Atabek O, Šindelka M and Moiseyev N 2009 *Phys. Rev. Lett.* **103** 123003
[31] Berry M V and Uzdin R 2011 *J. Phys. A: Math. Theor.* **44** 435303
[32] Milburn T J, Doppler J, Holmes C A, Portolan S, Rotter S and Rabl P 2015 *Phys. Rev. A* **92** 052124
[33] Zhang X, Wang S, Hou B and Chan C T 2018 *Phys. Rev. X* **8** 021066
[34] Li A, Dong J, Wang J, Cheng Z, Ho J S, Zhang D, Wen J, Zhang X, Chan C T, Alù A, Qiu C W and Chen L 2020 *Phys. Rev. Lett.* **125** 187403
[35] Liu W, Wu Y, Duan C, Rong X and Du J 2021 *Phys. Rev. Lett.* **126** 170506
[36] Yu F, Zhang X, Tian Z, Chen Q and Sun H 2021 *Phys. Rev. Lett.* **127** 253901
[37] Chen W, Abbasi M, Joglekar Y N and Murch K W 2021 *Phys. Rev. Lett.* **127** 140504
[38] Ren Z, Liu D, Zhao E, He C, Pak K K, Li J and Jo G B 2022 *Nat. Phys.* **18** 385
[39] Shu X, Li A, Hu G, Wang J, Alù A and Chen L 2022 *Nat. Commun.* **13** 2123
[40] Chen W, Abbasi M, Ha B, Erdamar S, Joglekar Y N and Murch K W 2022 *Phys. Rev. Lett.* **128** 110402
[41] Schumer A, Liu Y G N, Leshin J, Ding L, Alahmadi Y, Hassan A U, Nasari H, Rotter S, Christodoulides D N, LiKamWa P and Khajavikhan M 2022 *Science* **375** 884
[42] Am-Shallem M, Kosloff R and Moiseyev N 2015 *New J. Phys.* **17** 113036
[43] Minganti F, Miranowicz A, Chhajlany R W and Nori F 2019 *Phys. Rev. A* **100** 062131
[44] Minganti F, Miranowicz A, Chhajlany R W, Arkhipov I I and Nori F 2020 *Phys. Rev. A* **101** 062112
[45] Kumar P, Snizhko K and Gefen Y 2021 *Phys. Rev. A* **104** L050405
[46] Xie C, Sun K, Wu K, Li C, Guo G, Yi W and Xiang G 2024 *Sci. Bull.* **70** 3345
[47] Sun K and Yi W 2024 *AAPPS Bull.* **34** 22
[48] Carr C, Ritter R, Wade C G, Adams C S and Weatherill K J 2013 *Phys. Rev. Lett.* **111** 113901
[49] Marcuzzi M, Levi E, Diehl S, Garrahan J P and Lesanovsky I 2014 *Phys. Rev. Lett.* **113** 210401
[50] Melo N R, Wade C G, Šibalić N, Kondo J M, Adams C S and Weatherill K J 2016 *Phys. Rev. A* **93** 063863
[51] Šibalić N, Wade C G, Adams C S, Weatherill K J and Pohl T 2016 *Phys. Rev. A* **94** 011401
[52] Ding D, Busche H, Shi B, Guo G and Adams C S 2020 *Phys. Rev. X* **10** 021023
[53] Wadenpfuhl K and Adams C S 2023 *Phys. Rev. Lett.* **131** 143002
[54] Wu X, Wang Z, Yang F, Gao R, Liang C, Tey M K, Li X, Pohl T and You L 2024 *Nat. Phys.* **20** 1389
[55] Wang H, Assawaworrarit S and Fan S 2019 *Opt. Lett.* **44** 638
[56] Bai K, Fang L, Liu T R, Li J Z, Wan D and Xiao M 2023 *Natl. Sci. Rev.* **10** nwac259
[57] Li Z, Li C, Xu G, Chen W, Xiong Z, Jing H, Ho J S and Qiu C W 2023 *Sci. Adv.* **9** eadi0562